Torque Improvement in Dual *M*-Phase Permanent-Magnet Machines by Phase Shift for Electric Ship Applications

Yuhua Sun, Wenxiang Zhao, *Senior Member, IEEE*, Jinghua Ji, Junqiang Zheng, and Yu Cheng

***Abstract*—This paper proposes a design technique for electric ship traction machines to achieve high torque density and low torque ripple by adopting dual *m*-phase windings with an appropriate phase shift. Firstly, the general relationship between the slot number and the phase number for dual *m*-phase windings is investigated. Secondly, the uniform analytical expressions of torque with different phase shifts are derived. Also, the optimal phase shift angle is summarized from the perspective of improving torque performance. Then, the 48-slot and 22-pole permanent-magnet machines for electric ship with different windings configurations are designed. The finite-element method is used to calculate their electromagnetic performances, such as back electromotive force, torque capability, stator magnetic motive force and radial force. Finally, some experiments on the prototype machine for electric ship are carried out for validation.**

***Index Terms*—Dual *m*-phase windings, electric ship, permanent-magnet machine, phase shift, torque.**

I. Introduction

With increasing concern on energy security and environmental impacts, electric ships have been paid much expectation [1]–[3]. Significant works on the characteristics and design criteria of electric ship applications have been presented in [4]–[6], revealing that the applications possess low-speed and high-torque, high power density, high efficiency and reliability, low vibration and noise. In the meantime, the permanent-magnet (PM) machines adopt dual *m*-phase windings configurations can offer the merits of high windings factor, low stator magnetic motive force (MMF) harmonic components and high reliability, this can be a promising candidate for electric ship applications [7]. The electric ship applications require smooth torque because high torque ripple will result in unacceptable vibration, acoustic noise, and poor position and speed control [8]–[10].

At present, many published literatures have investigated torque ripple reduction in PM machines. Skewing stator slots or rotor poles, reshaping magnets and asymmetry magnets were widely used to reduce torque ripple [11]–[13]. In [14], the shapes of stator teeth and slot-opening were optimized to suppress torque ripple. To sum up, these methods are aimed at reducing torque ripple by adjusting machine topologies, which not only result in difficulty in machine manufacture, but also inevitably lower torque capability.

It is well known that as the phase number increases, the torque ripple can be reduced inherently, without sacrificing torque capability [15]. Currently, the dual 3-phase windings configuration was widely studied [16]–[18]. It has been indicated that the configuration with 30° phase shift has larger torque density and lower torque ripple than the traditional 3-phase windings ones. In addition, a nonconventional 15° angle displacement between the adjacent windings set was proposed in [19]. Besides, the star-delta hybrid connection to improve torque capability was proposed in [20] and [21]. However, this method requires asymmetric turn number and increases the complexity of the windings configuration. In [22] and [23], a dual 3-phase asymmetric stator windings configuration was adopted in a new multiphase PM machine, which offers low torque ripple and high torque density. However, this windings configuration requires a specific slot-pole combination. The effects of phase shift between multiple multiphase windings in flux-switching PM machines were investigated in [24]. In terms of reducing torque ripple, the optimal phase shift for multiple multiphase windings was summarized. However, this work did not concern the effect of current harmonics on torque performance. In [25] and [26], the influences of the current harmonics on torque performance were investigated, revealing that the torque can be improved by current harmonics injection. However, these researches focus on low order current harmonics to a large extent. In [27] and [28], the phase shift was adopted by a multilayer winding configuration to suppress the torque ripple and stator MMF harmonic components. However, this method causes some reduction in the windings factor of the torque-producing MMF component. To sum up, the existing papers mainly focus on the dual 3-phase windings configuration, and most of them adopt 30° angle displacement. Other dual multi-phase windings configurations with different phase shifts are rarely involved. The main contribution of this paper is to investigate and compare the torque performance of the dual *m*-phase windings with all possible phase shifts, in which the current harmonics can be considered.

Manuscript received June 4, 2019; revised November 1, 2019, March 31, 2020, and June 1, 2020; accepted June 17, 2020. Date of publication June 23, 2020; date of current version October 13, 2020. This work was supported in part by the National Natural Science Foundation of China under Grants 51991383 and 51777090, in part by the Key Research and Development Program of Jiangsu Province under Grant BE2018107, and in part by the Priority Academic Program Development of Jiangsu Higher Education Institutions. The review of this article was coordinated by Dr. C. Liu. *(Corresponding author: Wenxiang Zhao.)*

The authors are with the School of Electrical and Information Engineering, Jiangsu University, Zhenjiang 212013, China (e-mail: 1714034249@qq.com; zwx@ujs.edu.cn; jjh@ujs.edu.cn; 2289832202@qq.com; 3130501041@stmail.ujs.edu.cn).

Digital Object Identifier 10.1109/TVT.2020.3004161

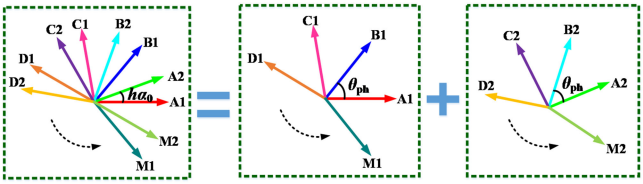

Fig. 1. Phase shift between adjacent windings set in dual m-phase windings configurations.

This paper is organized as follows. In Section II, the general relationship between the slot number and the phase number for the dual m-phase windings configurations are presented. Then, the complete analytical expressions of torque, excited by sinusoidal and non-sinusoidal currents, are derived to reveal the principle between optimal phase shift and torque performance. In Section III, the 48-slot and 22-pole PM machines are designed and their performances are comprehensively calculated by using the finite-element method to verify the theoretical analysis results. In Section IV, some experiments on the prototype machine are carried out for validation. Finally, conclusions are drawn in Section V.

II. Dual m-Phase Windings Configurations and Torque Characteristics

The traditional symmetric m-phase windings PM machines suffer from low windings factor and large torque ripple, which is unacceptable for electric ship applications. To overcome these shortcomings, PM machines can be connected to dual m-phase windings. The key of this technique is to determine the optimal phase shift α_{op}. In this section, the relationship between the slot number and the phase number will be investigated. Then, the appropriate phase shift for the dual m-phase windings will be discussed.

The dual m-phase windings configurations and the phase shifts are shown in Fig. 1, where A1, B1, C1, …, M1 refer to the phases of the first windings set, A2, B2, C2, …, M2 refer to the phases of the second windings set. θ_{ph} is the phase difference for each windings set. The slot-pitch angle α_0 and spatial phase difference of two windings sets α should satisfy [20]

$$\alpha = h\alpha_0 = \frac{2\pi}{k_1 m} \tag{1}$$

where m is the phase number (m>1), h is the slot-pitch number. Besides, k_1 is constant and constrained by phase shift α. Then, by substituting the expression of slot-pitch angle α_0 into (1) [20], the relationship between the slot number and the phase number can be obtained, which is appropriate for the dual m-phase windings with different phase shifts. The relation equation can be written as

$$Z = mk_1 h \tag{2}$$

where Z is the slot number, and the unit machine number is 1. The slot number and the phase number for dual m-phase windings are limited and their relationship should meet $Z = mk_1 h$. It is worth noting that $k_1 h$ should be an even number. The common slot number for the dual m-phase windings with different phase shifts are listed in Table I. The oblique line indicates that it is not suitable for dual m-phase windings configuration. Specifically, dual 3-phase windings configuration is adopted and the phase shift α is 7.5°, 15°, 30°, and 60°, respectively. Namely, m equals to 3 and k_1 equals to 16, 8, 4, and 2, respectively. In the case of h = 1, the slot number of unit machine which can satisfy the above windings configurations is 48, 24, 12 and 6, correspondingly.

TABLE I
Slot Number for Dual m-Phase Windings With Different Phase Shifts

Phase shifts	h=1	h=2	h=3	h=4	…
$2\pi/m$	/	$2m$	/	$4m$	…
π/m	$2m$	$4m$	$6m$	$8m$	…
$2\pi/3m$	/	$6m$	/	$12m$	…
$\pi/2m$	$4m$	$8m$	$12m$	$16m$	…
…	…	…	…	…	…

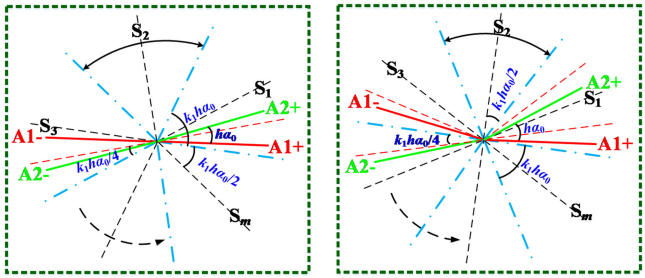

Fig. 2. Equivalent slot electric potential star diagram for dual m-phase windings. (a) m is odd or 2. (b) m is even except 2.

Fig. 2 is the equivalent slot electric potential star diagram for dual m-phase windings. The star of slots is divided into S_1, S_2, …, S_m. Two sectors are assigned to each phase, and they are referred to as positive (e.g., labeled A1+) and negative sectors (e.g., labeled A1−). It is well known that high windings factor means great potential for increasing torque density. When the slot number in unit machine satisfies $Z = mk_1 h$, the slot number per phase Z_m is $k_1 h/2$. When m is odd or 2, the slot number per phase Z_m is twice the slot-pitch number h, which can offer the largest fundamental windings factor than other competing phase shifts. Correspondingly, the slot number per phase Z_m should be equal to slot-pitch number h for m is even except 2. It can be summarized as

$$\begin{cases} k_1 = 4 & m \text{ is odd or } 2 \\ k_1 = 2 & m \text{ is even except } 2 \end{cases} \tag{3}$$

A. Torque With Ideal Sinusoidal Current

The torque of surface-mounted PM machines only has PM torque component, and low cogging torque can be obtained by selecting proper slot-pole combinations. In this case, the torque ripple of the surface-mounted PM machines mainly results from the PM torque. It is worth noting that different phase shifts cannot influence the cogging torque. Conversely, the phase shifts greatly affect the PM torque.

When the back electromotive force (back-EMF) is symmetrical and has no even order harmonics, the back-EMF can be expressed as

$$e_{k_2}(\omega t) = \sum_{v=1,3,5\ldots} E_v \cdot \sin\{v[\omega t - (k_2-1)\alpha] + \varphi_{vk_2}\} \quad (4)$$

where ω is the electric angular frequency, t is the time, v is the back-EMF harmonics order, and k_2 ($k_2 = 1, 2$) denotes the k_2^{th} m-phase windings set. E_v is the amplitude of the v^{th} back-EMF harmonic, and φ_{vk2} is the phase angle of the v^{th} back-EMF harmonic of the k_2^{th} m-phase windings set. Due to the symmetrical distribution, the back-EMF of the k_2^{th} m-phase windings set can be written as

$$\begin{cases} e_{Ak_2} = e_{k_2}(\omega t) \\ e_{Bk_2} = e_{k_2}(\omega t - \theta_{ph}) \\ e_{Ck_2} = e_{k_2}(\omega t - 2\theta_{ph}) \\ \ldots\ldots \end{cases} \quad (5)$$

where θ_{ph} equals to $2\pi/m$ (m>2) and $\pi/2$ ($m = 2$), respectively. Based on the same analytical method, when using $i_d = 0$ control strategy, the current expression can be derived [29]. Therefore, the torque produced by the first windings set can be obtained as

$$\begin{aligned} T_{e1}(\omega t) &= \frac{1}{n_{me}}(e_{A1}i_{A1} + e_{B1}i_{B1} + e_{C1}i_{C1} + \ldots\ldots e_{M1}i_{M1} \\ &= \frac{1}{2n_{me}} \sum_{v=1,3\ldots} \sum_{j=1}^{m-1} E_v I_{\max}\{\cos[(v-1)\omega t - (v-1) \\ &\quad \times (j-1)\theta_{ph} + (\varphi_{v1} - \varphi_{11})] - \cos[(v+1)\omega t \\ &\quad - (v+1)(j-1)\theta_{ph} + (\varphi_{v1} + \varphi_{11})]\} \end{aligned} \quad (6)$$

where j ($j = 1, 2, 3, \ldots, m$) is the phase sequence, n_{me} is the mechanical rotor angular speed, $I_{\max}$ is the amplitude of ideal sinusoidal current. According to (6), the v^{th} back-EMF harmonic contributes to the generation of torque ripple only if $(v\pm1) = ml$ ($l = 1, 2, 3, \ldots$). It should be pointed out that the average torque generation in the case of $v = 1$ for the sinusoidal current. Thus, the back-EMF harmonics orders, which interact with the sinusoidal current to generate torque ripple, can be expressed as

$$v = \begin{cases} 2ml \pm 1 & m \text{ is odd or } 2 \\ ml \pm 1 & m \text{ is even except } 2 \end{cases} \quad (7)$$

The torque for the second symmetrical winding T_{e2} can be obtained by replacing ωt in (6) with (ωt-α). Consequently, the total electromagnetic torque T_e can be given by

$$\begin{aligned} T_e(\omega t) = T_{e1}(\omega t) + T_{e2}(\omega t) &= \sum_{n=0,2\ldots} \sum_{j=1}^{m-1} T_n \\ &\times \cos\left\{n\left[\omega t - (j-1)\theta_{ph} - \frac{\alpha}{2}\right] + \varphi_n\right\} \cos\left(\frac{n\alpha}{2}\right) \end{aligned} \quad (8)$$

where n is the torque harmonics order, and T_n is the amplitude of the n^{th} torque harmonics. It is worth noting that the torque performance of 3-phase windings configuration is identical to the dual 3-phase windings configuration with $\alpha = 0°$ one. Generally,

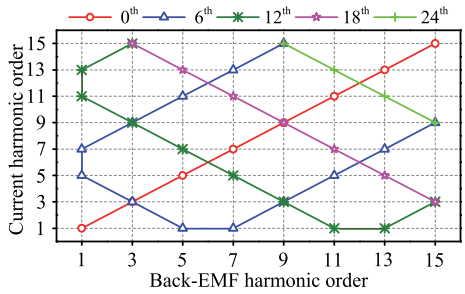

Fig. 3. Relationship between back-EMF harmonic order and current harmonic order generating torque for each symmetrical 3-phase windings set.

the most significant torque harmonics are the $(2m)^{\text{th}}$ (m is odd or 2) and the m^{th} (m is even except 2) components. According to (8), the n^{th} torque harmonics can be eliminated when it satisfies $\cos(n\alpha/2) = 0$. In order to minimize torque ripple, the most significant harmonic should be eliminated. In the meantime, the maximum fundamental windings factor is required in order to increase the torque density. Thus, the optimal phase shift α_{op} is defined as the angle which can eliminate the most significant torque harmonic. Also, the maximum fundamental windings factor can be obtained. Based on (3) and (8), it can be concluded as

$$\alpha_{op} = \begin{cases} \frac{\pi}{2m} & m \text{ is odd or } 2 \\ \frac{\pi}{m} & m \text{ is even except } 2 \end{cases} \quad (9)$$

B. Torque With Non-Sinusoidal Current

In fact, the real current contains some harmonic components, so it is necessary to determine the influence of the current harmonics on torque performance. When the phase current is symmetrical, it can be written as [31]. Therefore, the torque of first windings set with current harmonics can be written as

$$\begin{aligned} T_{e1}(\omega t) &= \frac{1}{n_{me}}(e_{A1}i_{A1} + e_{B1}i_{B1} + e_{C1}i_{C1} + \ldots\ldots e_{M1}i_{M1}) \\ &= \sum_{v=1,3\ldots} \sum_{i=1,3\ldots} \sum_{j=1}^{m-1} \frac{E_v I_\mu}{2n_{me}}\{\cos[(v-\mu)\omega t - (v-\mu) \\ &\quad \times (j-1)\theta_{ph} + (\varphi_{v1} - \varphi_{\mu 1})] - \cos[(v+\mu)\omega t \\ &\quad - (v+\mu)(j-1)\theta_{ph} + (\varphi_{v1} + \varphi_{\mu 1})]\} \end{aligned} \quad (10)$$

where μ is the current harmonics order, I_μ is the amplitude of the μ^{th} current harmonic, and $\varphi_{\mu 1}$ is the phase angle of the μ^{th} current harmonic of the first m-phase windings set. According to (10), it can be concluded that the v^{th} back-EMF harmonic interact with the μ^{th} current harmonic contributes to the torque ripple generation, when $(v\pm\mu) = ml$ is satisfied. Therefore, the back-EMF harmonics order, which interact with the current harmonics to generate torque ripple, can be written as

$$v = \begin{cases} 2ml \pm \mu & m \text{ is odd or } 2 \\ ml \pm \mu & m \text{ is even except } 2 \end{cases} \quad (11)$$

Specifically, Fig. 3 reveals the relationship between the back-EMF harmonic order and the current harmonic order generating

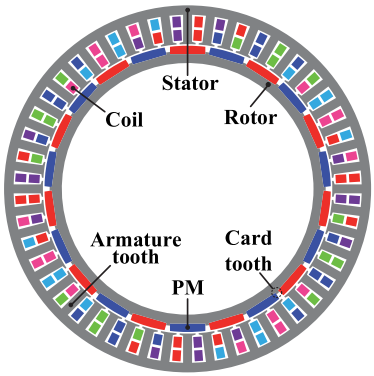

Fig. 4. Cross section of 48-slot and 22-pole PM machine.

torque of single 3-phase windings set, in which the different color curves represent different torque harmonics order as shown in legend. It can be seen that torque harmonic components is $(6l)^{\text{th}}$. Moreover, the 6^{th} harmonic is the lowest order of main harmonics, which is the first main harmonics for each symmetrical 3-phase windings set. The amplitude of the harmonics decreases with the harmonic order. Therefore, the 6^{th} torque harmonic elimination is the key to reduce torque ripple for 3-phase winding machines.

Then, by substituting (10) into (8), it can be known that torque harmonics can be eliminated when it satisfies $\cos((v\pm\mu)\alpha/2) = 0$. Compared with the sinusoidal current, the current harmonics do not change torque harmonics order, but influence the original contents. Moreover, the most significant harmonic order is consistent with the sinusoidal current, and the current harmonics cannot cause changes in windings factor. Hence, the conclusion of (9) is also suitable for the non-sinusoidal current case. To be specific, the $(6c)^{\text{th}}$ ($c = 1, 3, 5, \ldots$) torque harmonics can be cancelled for dual 3-phase windings when $\alpha = 30°$, while the maximum fundamental windings factor is obtained.

In addition, the optimal phase shift can eliminate torque ripple caused by the specific current harmonics. This technique can be used to improve the torque density of the electric ship traction machines without generating additional torque ripple by injecting the current harmonics [29]–[31].

III. Simulation and Evaluation

For a clear explanation, the surface mounted PM machine for electric ship having 48-slot and 22-pole combination is chosen as example, in which the vibration and noise performance are considered [32]. The cross section of this PM machine is shown in Fig. 4. Its main specifications are listed in Table II. As can be seen, the surface mounted PMs are fixed by card teeth. The height and width of card teeth are small, hence the reluctance torque can be almost neglected in this topology. The two-layer fractional slot distributed windings are adopted for the purpose of high windings factor. Moreover, the greatest common divisor of the slot number and pole number is selected as 2 to reduce cogging torque. Based on this slot-pole combination, the dual 3-phase windings, dual 4-phase windings and dual 6-phase windings can be adopted. In this section, the case of $m = 3$ is analyzed and verified. It is worth emphasizing that the analysis method in this paper is universal, which is not limited to dual 3-phase windings. Besides, electromagnetic performances of the prototype PM machines with different phase shifts are compared by using the finite-element method, such as back-EMF, torque capability, stator MMF harmonic and radial force.

TABLE II
Main Specifications of Prototype Machines

Items	Values
Rated speed (r/min)	200
Rated current I (A)	9.3
Outer diameter of stator D_{so} (mm)	350
Inner diameter of stator D_{si} (mm)	276
Inner diameter of rotor D_{ri} (mm)	240
Air-gap length g (mm)	1.5
Axial length L (mm)	150
Tooth width d_1 (mm)	8.5
Thickness of PM h_{pm} (mm)	8
Polar-arc coefficient of PM α_{pm}	0.87
Turns per phases N	30
Remanence of PM B_r (T)	1.1
PM material	Smco32

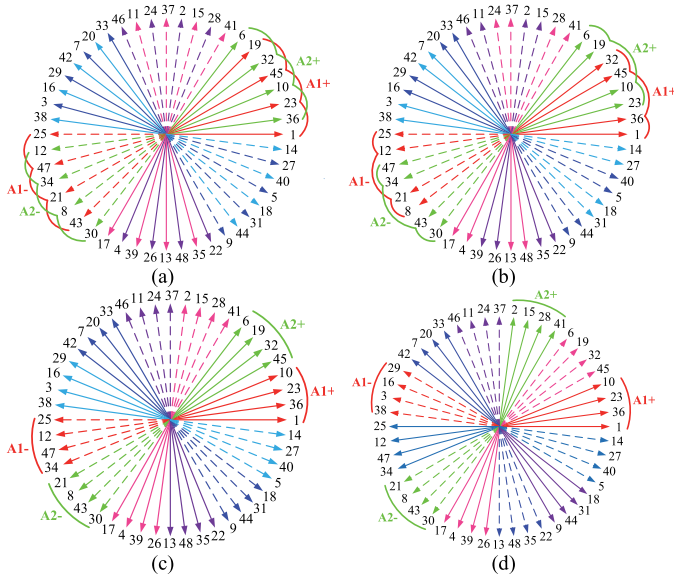

Fig. 5. Slot electric potential star diagram for dual 3-phase windings configurations. (a) $\alpha = 7.5°$. (b) $\alpha = 15°$. (c) $\alpha = 30°$. (d) $\alpha = 60°$.

A. Windings Factor and No-Load Back-EMF

Based on (1) and (2), the 48-slot and 22-pole PM machine can be connected to the dual 3-phase windings with α equals to 7.5°, 15°, 30°, and 60°, respectively, as shown in Fig. 5. The positive sectors of phases A1 and A2 are labeled as A1+, A2+. Similarly, for the negative sectors, the letters A1- and A2- are used. The number of spokes in each sector is 4, and the slot-pitch number h is 1, 2, 4 and 8, corresponding to phase shift α equals to 7.5°, 15°, 30°, and 60°, respectively. According to the general formulation of windings factor [19], [33], the

TABLE III
WINDINGS FACTORS FOR DUAL 3-PHASE WITH DIFFERENT PHASE SHIFTS

α	k_{dv}	$v=p$	$v=3p$
0°	$\lvert\sin^2(\frac{2v\pi}{Z})\cos(\frac{4v\pi}{Z})\cos(\frac{13v\pi}{Z})\rvert$	0.947	0.592
7.5°	$\lvert\sin^2(\frac{2v\pi}{Z})\cos(\frac{4v\pi}{Z})\rvert$	0.949	0.604
15°	$\lvert\sin(\frac{2v\pi}{Z})\cos(\frac{4v\pi}{Z})\cos(\frac{13v\pi}{Z})\rvert$	0.956	0.641
30°	$\lvert\sin^2(\frac{2v\pi}{Z})\cos(\frac{13v\pi}{Z})\rvert$	0.981	0.837
60°	$\lvert\sin^2(\frac{2v\pi}{Z})\cos(\frac{4v\pi}{Z})\cos(\frac{13v\pi}{Z})\rvert$	0.947	0.592

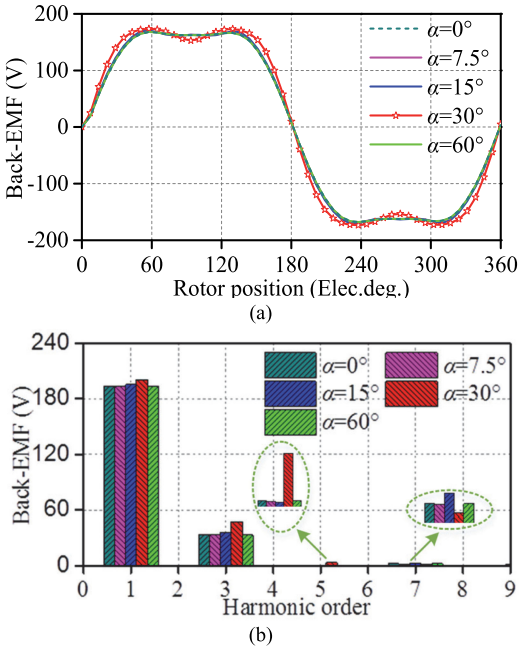

Fig. 6. Comparison of no-load back-EMF of dual 3-phase windings configurations. (a) Waveform. (b) Spectrum.

main windings factor at different phase shifts can be calculated as given in Table III. Besides, this machine will be connected to the dual 4-phase windings with α equals to 7.5°, 22.5°, and 45°, respectively. The fundamental windings factor is calculated as 0.893, 0.911, and 0.967, correspondingly. Obviously, the maximum fundamental windings factor can be obtained when the optimal phase shift is adopted.

Fig. 6 shows the waveform and space harmonic spectrum of the back-EMFs with different phase shifts at the same rotation speed. In one electrical period, the fundamental order is the 1st. The torque harmonic generated by the 5th, 7th back-EMF harmonics are eliminated when $\alpha = 30°$. In order to show the influences of phase shifts on electromagnetic performances clearly, the results of the $\alpha = 0°$ windings configuration are added. It can be seen that the $\alpha = 30°$ windings configuration has larger fundamental harmonic magnitude than that of other phase shifts windings. This is because it has maximum windings factor. Although the 3rd back-EMF harmonic amplitude of the $\alpha = 30°$ windings is higher than other competing phase shifts windings one, it does not contribute to torque ripple in the case of the sinusoidal current. This feature means great potential for increasing torque density by the 3rd current harmonic injection,

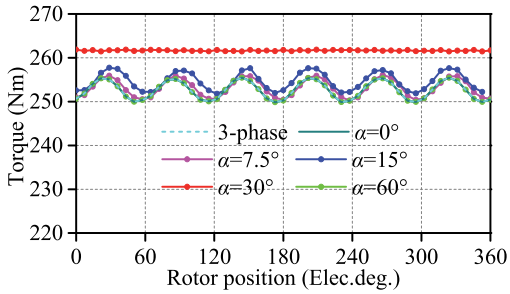

Fig. 7. Waveforms of total torque in different windings configurations with ideal sinusoidal current.

which will be elaborated in Section III-C. The analysis method is also applicable to the dual even-phase windings.

B. Torque With Ideal Sinusoidal Current

Fig. 7 presents the torque waveforms of different windings configurations with ideal sinusoidal current. Obviously, the torque performances of 3-phase windings and the $\alpha = 0°$ windings configurations are identical to the $\alpha = 60°$ windings configuration. Hence, the first second windings configuration will not be discussed later. The phase shift not only affects the amplitude of average torque, but also affects torque ripple. Fig. 8 shows the torque waveform of each 3-phase windings set with different phase shifts. As can be seen, the most significant torque harmonic order is the 6th for each winding set, that is, the torque period is 60° in an electrical period. Moreover, the torque angle displacement between two windings sets equals phase shift α. Therefore, the torque phase of two windings sets are compensated when $\alpha = 30°$ as shown in Fig. 8(c). Fig. 9 compares the spectrum of total torque with different phase shifts. It can be known that the 6th torque harmonic can be completely eliminated when $\alpha = 30°$, and the average torque is maximum. This is the optimal phase shift for dual 3-phase windings. Similarly, when this machine is connected to the dual 4-phase windings with $\alpha = 45°$, the torque ripple can be smaller than other competing phase shifts windings one.

For the purpose of further verifying the generality of the optimal phase shift conclusion, other three PM machines are designed. The slot-pole combinations include 16-slot and 12-pole, 20-slot and 14-pole, 24-slot and 20-pole. They are equipped with the dual 4-phase windings configuration, the dual 5-phase windings configuration and the dual 6-phase windings configuration, respectively, while the optimal phase shift is adopted. In order to prove the advantages of optimal phase shift in torque performance, the $\alpha = 0°$ windings configurations are selected for evaluation. Figs. 10–12 show the slot electric potential star diagram of the three machines. According to [33], the fundamental windings factor can be calculated as 0.854 and 0.924 for 16-slot and 12-pole, respectively. Correspondingly, the fundamental windings factor is 0.880 and 0.891 for 20-slot and 14-pole, 0.933 and 0.966 for 24-slot and 20-pole. The torque waveforms of the three machines with optimal phase shift are highlighted with dotted box in Fig. 13. The red and blue curves represent the torque waveforms of the first and second

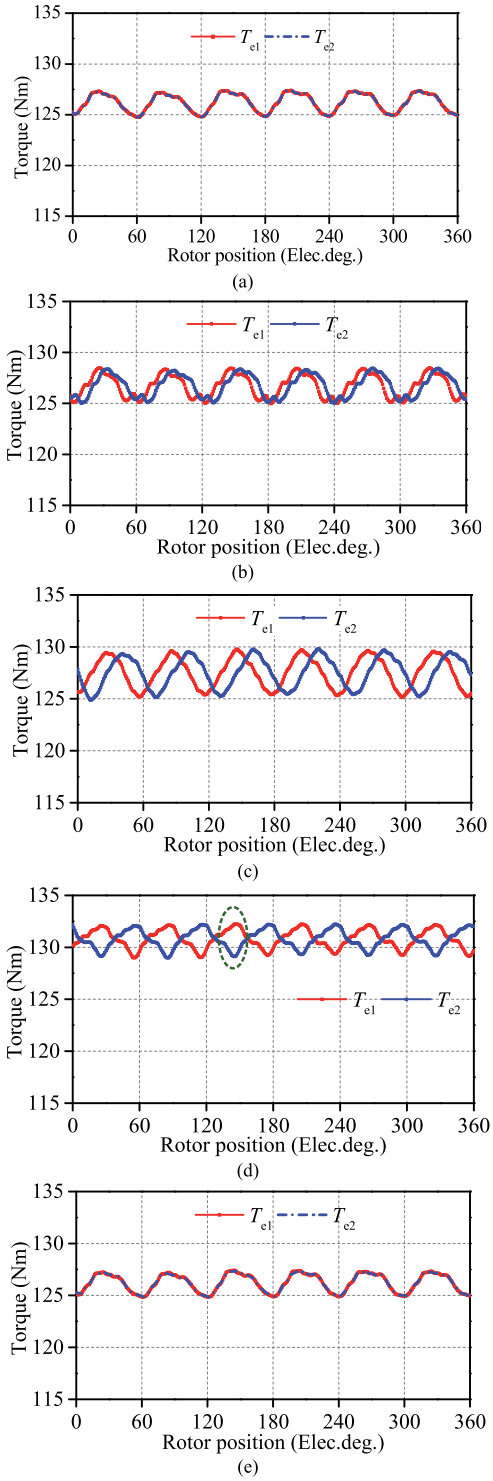

Fig. 8. Torque separation in dual 3-phase windings configurations. (a) $\alpha = 0°$. (b) $\alpha = 7.5°$. (c) $\alpha = 15°$. (d) $\alpha = 30°$. (e) $\alpha = 60°$.

windings set respectively. Obviously, the torque waveforms of two windings sets are mutual compensated, thereby, the most significant torque harmonic can be completely eliminated. Further, Fig. 13 indicates the total torque spectrum comparison of the three machines. It is known that the $(4c)^{\text{th}}$, $(10c)^{\text{th}}$, $(6c)^{\text{th}}$ torque harmonics are eliminated respectively in the 16-slot and

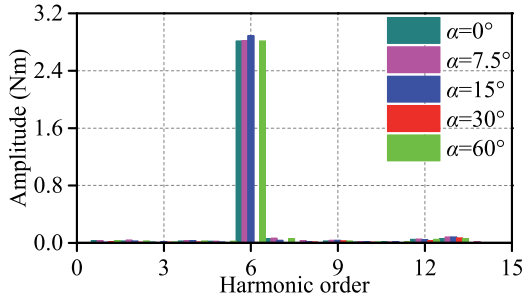

Fig. 9. Spectrum comparison of total torque in dual 3-phase windings configurations.

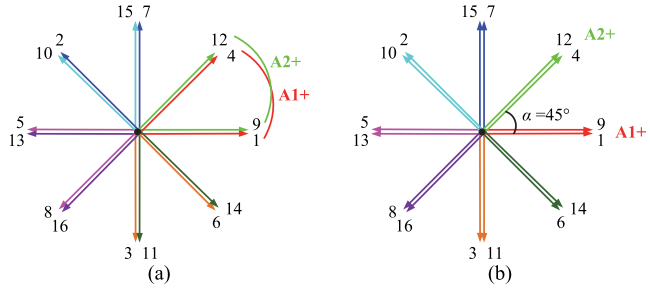

Fig. 10. Slot electric potential star diagram of 16-slot and 12-pole. (a) $\alpha = 0°$. (b) $\alpha = 45°$.

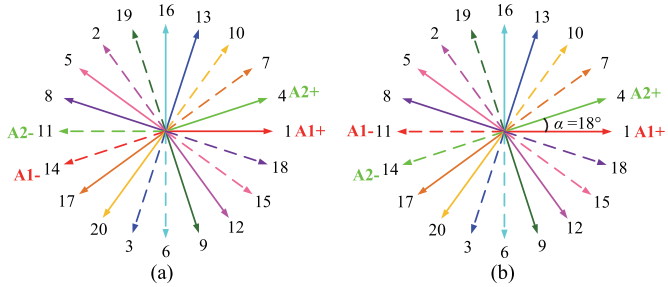

Fig. 11. Slot electric potential star diagram of 20-slot and 14-pole. (a) $\alpha = 0°$. (b) $\alpha = 18°$.

12-pole, 20-slot and 14-pole, and 24-slot and 20-pole machines by adopting the optimal phase shift, which are consistent with the analysis results in Section II.

C. Torque With Non-Sinusoidal Current

Fig. 14 shows the average torque and torque ripple when the rectangular current is applied. It is worth noting that the fundamental current amplitude of the rectangular current equals to the sinusoidal current amplitude $I_{\max}$. Since the presence of the current harmonics, the average torque and torque ripple are greatly improved. Fig. 15 describes the spectrum comparison of the total torque in the dual 3-phase windings with the rectangular current. It can be seen that the $(6c)^{\text{th}}$ torque harmonic components can be eliminated when $\alpha = 30°$. Similarly, the $(24c)^{\text{th}}$ and the $(12c)^{\text{th}}$ torque harmonic components can be cancelled in the case of the $\alpha = 7.5°$ windings configuration and the α

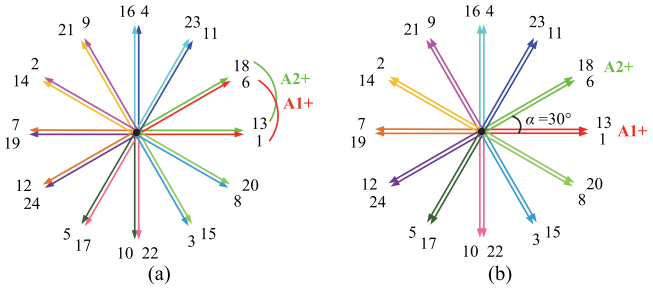

Fig. 12. Slot electric potential star diagram of 24-slot and 20-pole. (a) $\alpha = 0°$. (b) $\alpha = 30°$.

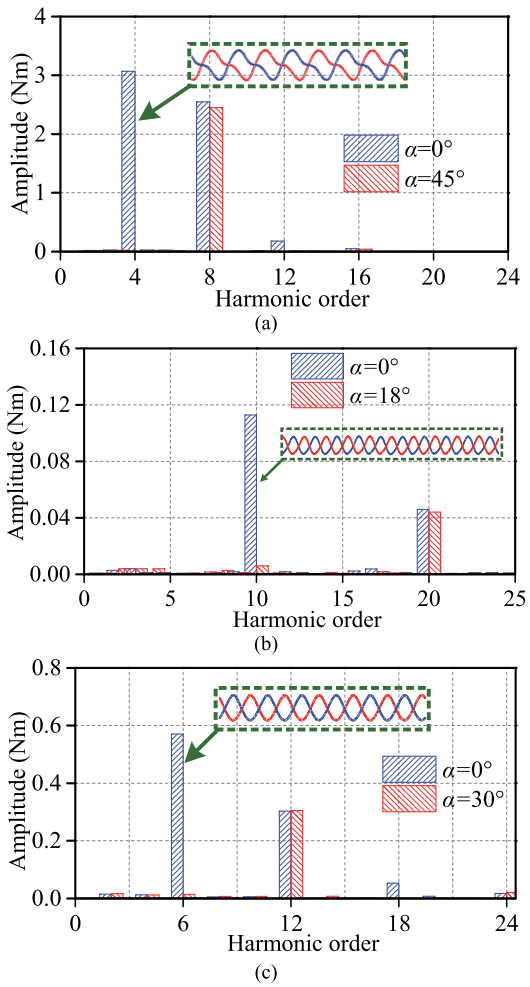

Fig. 13. Spectrum comparison of total torque. (a) 16-slot and 12-pole. (b) 20-slot and 14-pole. (c) 24-slot and 20-pole.

$= 15°$ windings configuration, respectively. However, the $\alpha = 60°$ windings configuration cannot change the torque harmonics order. This proves that the advantage of $\alpha = 30°$ in torque performance is not limited to the sinusoidal current.

Additionally, the back-EMF amplitude of the harmonic orders higher than 3 can be ignored for this machine. This is a typical case of the 3rd current harmonic injection to improve torque density. The back-EMF of phase A1 can be simplified [31]. When the neutral point is provided, the 3rd current harmonic,

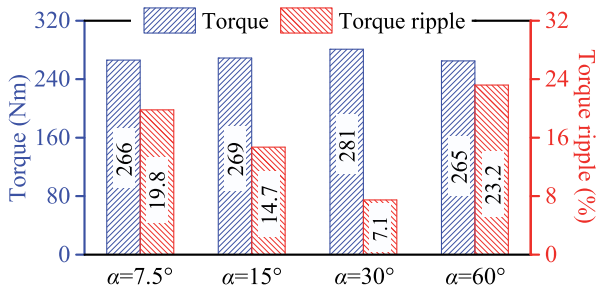

Fig. 14. Comparison of output torque and torque ripple in dual 3-phase windings configurations with rectangular current.

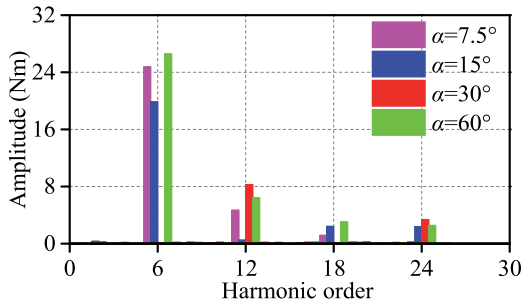

Fig. 15. Spectrum comparison of total torque in dual 3-phase windings configurations with rectangular current.

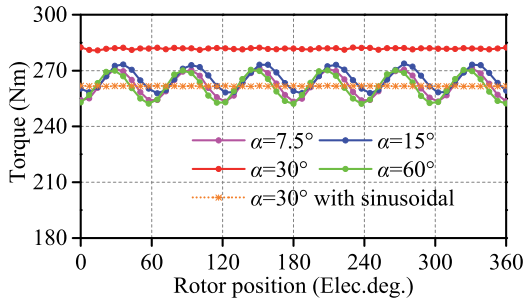

Fig. 16. Comparison of total torque waveform in dual 3-phase windings configurations with 3th-order current harmonic injection.

which interacts with 3rd back-EMF harmonic, can be used to improve the torque capability. The torque of the dual 3-phase windings in this case can be written as

$$T_e(\omega t) = \frac{3}{n_{me}}(E_1 I_1 + E_3 I_3) + T_{rip} \tag{12}$$

where the T_{rip} is total torque ripple. In order to have the same root mean square value as the sinusoidal current, I_1, I_3 and $I_{\max}$ meet $I_1^2 + I_3^2 = I_{\max}^2$. Therefore, the value of I_1 and I_3 can be calculated to obtain the maximum torque by [29]

$$\begin{cases} I_1 = I_{\max} / \sqrt{1 + \left(\frac{E_3}{E_1}\right)^2} \\ I_3 = \frac{E_3}{E_1} \cdot I_1 \end{cases} \tag{13}$$

In the case of the $\alpha = 30°$ windings, the 3rd current harmonic does not generate additional torque ripple. Namely, T_{rip} in (12) equals to 0. Fig. 16 compares the total torque waveform at different phase shifts with the 3rd current harmonic injection. It can

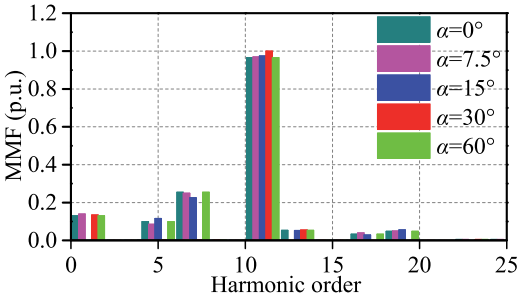

Fig. 17. Spectrum comparison of stator MMF harmonics content in dual 3-phase windings configurations with sinusoidal current.

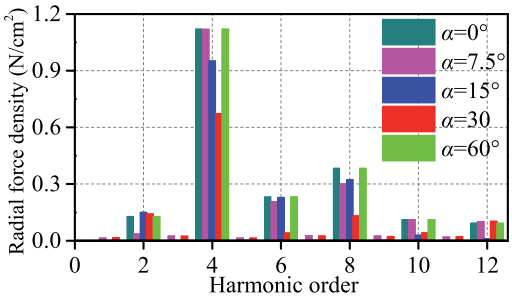

Fig. 18. Spectrum comparison of radial force harmonics in dual 3-phase windings configurations with sinusoidal current.

TABLE IV
ELIMINATION STATOR MMF HARMONICS ORDER (WITHIN 50)

Phase shifts	Elimination MMF harmonic order
α=0°	1,5,7,11,13,17,19,23,25,29,31,35,37,41,43,47,49…
α=7.5°	1,5,7,11,13,17,19,23,25,29,31,35,37,41,43,47,49…
α=15°	1,5,7,11,13,17,19,23,25,29,31,35,37,41,43,47,49…
α=30°	1,5,7,11,13,17,19,23,25,29,31,35,37,41,43,47,49…
α=60°	1,5,7,11,13,17,19,23,25,29,31,35,37,41,43,47,49…

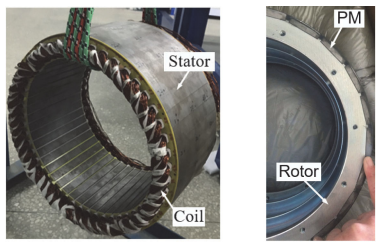

(a) (b)

Fig. 19. Prototype of the proposed 48-slot and 22-pole machine.

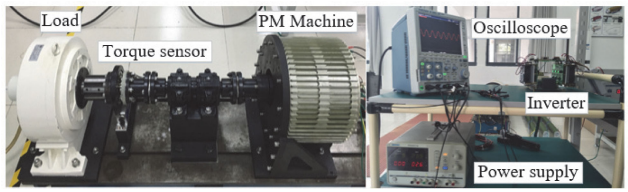

Fig. 20. Experimental platform.

be seen that the average torque increases by 8% approximately, compared with ideal sinusoidal current.

D. Stator MMF and Radial Force

The machine connects to the dual m-phase windings with the optimal phase shift not only has better torque performance than other competing phase shifts, but also has advantages in stator MMF harmonic components and radial force density. It should be noted that the analysis below is based on the ideal sinusoidal current.

The multiple 3-phase windings sets have been proposed to cancel out the stator MMF harmonic components [34]. It is known that the MMF harmonic will be eliminated when it satisfies

$$\theta_f = s(\beta_2 - \beta_1) + \alpha = \pm 180^\circ \pm 360^\circ l$$
$$\theta_b = s(\beta_2 - \beta_1) - \alpha = \pm 180^\circ \pm 360^\circ l \quad (14)$$

where s is the stator MMF harmonics order. θ_f represents the forward combined MMF harmonic phase shift, θ_b represents the backward combined MMF harmonic phase shift, and the (β_2-β_1) is determined by the slot electric potential star diagram. For prototype machines in the dual 3-phase windings, when the phase shift α is selected to be 7.5°, 15°, 30°, 60°, the β_2-β_1 becomes 97.5°, −165°, 30°, 60°, respectively.

Fig. 17 represents the normalized stator MMF harmonics spectrum of the dual 3-phase windings with different phase shifts, and the base value is the fundamental amplitude of the $\alpha = 30°$ windings configuration. It is obviously known that the $\alpha = 30°$ windings configuration eliminates some high content harmonics. Specifically, the reductions in stator MMF harmonics are listed in Table IV by the red font.

It is a common knowledge that the stator MMF harmonics reduction has profound influence on vibration, acoustic noise and eddy-current loss [32], [35]. Fig. 18 shows the spectrum comparison of the radial force harmonics in the dual 3-phase windings with different phase shifts. It is necessary to point out that the main 5th and 7th stator MMF harmonics are cancelled out when $\alpha = 30°$, which has important contribution to the 4th and 6th radial force harmonics, respectively. Additionally, the 17th and 19th stator MMF harmonics are eliminated, which is helpful for reducing the 8th and 10th radial force harmonics. To sum up, the main low order radial force harmonics are reduced, such as 4th, 6th, 8th and 10th. Although there is insignificant decrease in 2nd radial force harmonic, its content is less abundant.

IV. EXPERIMENTAL VALIDATION

In order to experimentally validate the theoretical analysis, the prototype PM machine with 48-slot and 22-pole has been built, as shown in Fig. 19. The prototype machine performance tests are conducted on an experiment platform as shown in Fig. 20, in which the machine adopts $i_d = 0$ control and provide load torque during tests. Fig. 21 shows the windings connection diagrams of 3-phase windings configuration and dual 3-phase windings configurations with $\alpha = 0°$ and $\alpha = 30°$, respectively. The characteristic is worth noting that the dual 3-phase windings configuration with $\alpha = 30°$ becomes 3-phase windings configuration when the outlet terminals of A1- and A2+ in series,

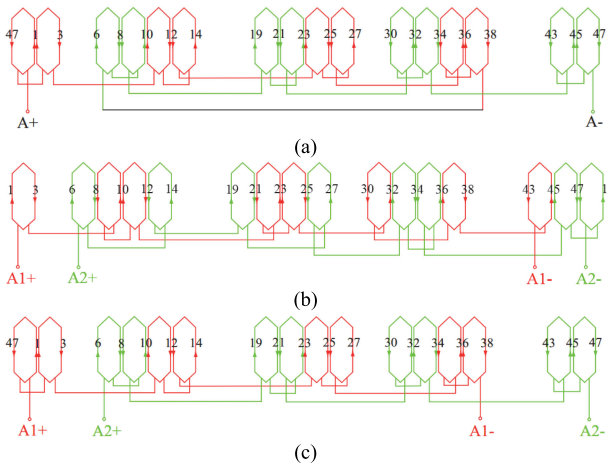

Fig. 21. The windings connection diagram. (a) 3-phase windings configuration. (b) Dual 3-phase windings configuration with $\alpha = 0°$. (c) Dual 3-phase windigns configuration with $\alpha = 30°$.

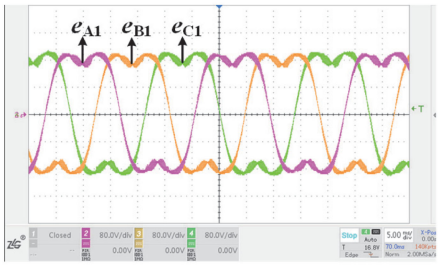

Fig. 22. Measured back-EMF of prototype machine at 200 r/min in dual 3-phase windings configuration with $\alpha = 30°$. (5 ms/div, 80 V/div).

B1- and B2+ in series, C1- and C2+ in series. The torque performance of 3-phase windings configuration is identical to the dual 3-phase windings configuration with $\alpha = 0°$ one. Hence, the following related experiments are based on the 3-phase windings configuration to show the torque characteristics of dual 3-phase windings configuration with $\alpha = 0°$.

Fig. 22 shows the measured back-EMFs of the dual 3-phase windings with $\alpha = 30°$ at 200 r/min, in which e_{A1}, e_{B1} and e_{C1} represent the back-EMF waveforms of phase A1, phase B1 and phase C1, respectively. It is worth mentioning that the back-EMF of the second windings set are not tested, which only has 30° phase difference relative to the first windings set ones. Furthermore, the measured and predicted results of the back-EMF waveform and corresponding harmonic analysis, for 3-phase windings configuration and dual 3-phase windings configuration with $\alpha = 30°$, are compared in Fig. 23 and Fig. 24. It can be seen that the measured fundamental component is about 2.5% lower than the predicted one. This is mainly due to the effect of lamination factor, end effect and manufacturing error. It is mentioned that the back-EMF results of dual 3-phase windings configuration with $\alpha = 0°$ is half of the 3-phase windings configuration ones.

Fig. 25 shows the measured torque waveforms of the $\alpha = 0°$ windings and the $\alpha = 30°$ windings configurations at 200 r/min,

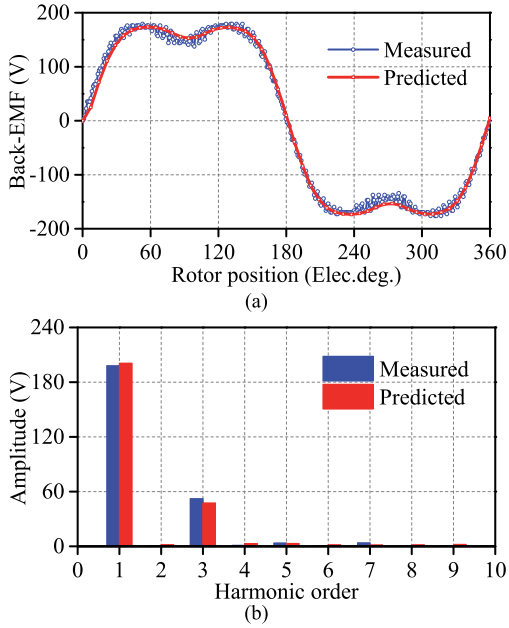

Fig. 23. Comparison of the measured and predicted A1 phase back-EMF in dual 3-phase windings configuration with $\alpha = 30°$. (a) Waveform. (b) Spectrum.

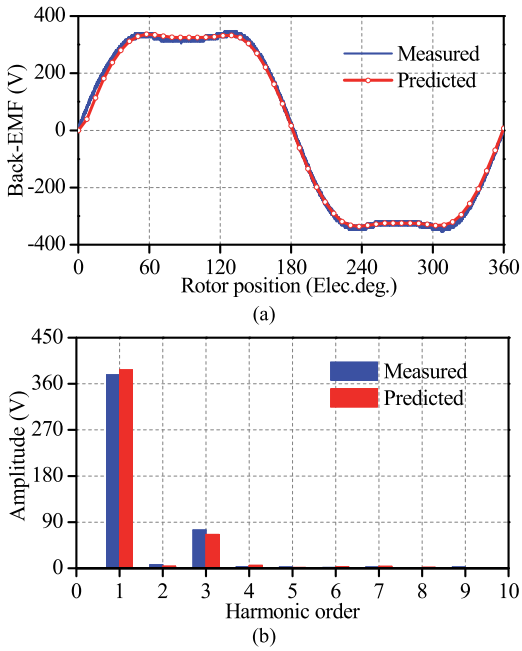

Fig. 24. Comparison of the measured and predicted A phase back-EMF in 3-phase windings configuration. (a) Waveform. (b) Spectrum.

and the measured current values are 10.8A and 10.3A respectively. Correspondingly, the predicted ones are 9.7A and 9.3A. The main reason is that the mechanical loss is not taken into account during the prediction. Fig. 26 compares the measured and predicted results of the torque waveform at 200 r/min. It is worth noting that the comparisons are based on the premise that the average torque is identical, that is, the current amplitudes are different in each case. The 30° configuration requires smaller current amplitude compared with its counterpart, which

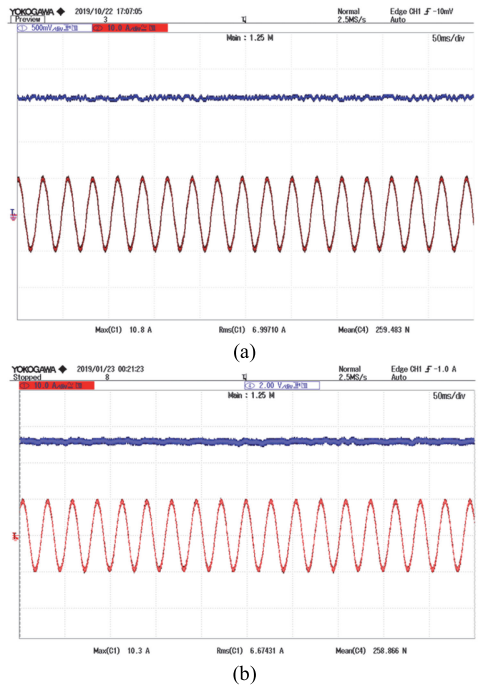

Fig. 25. Measured torque waveforms. (50 ms/div, 10 A/div). (a) The $\alpha = 0°$ windings configuration. (b) The $\alpha = 30°$ windings configuration.

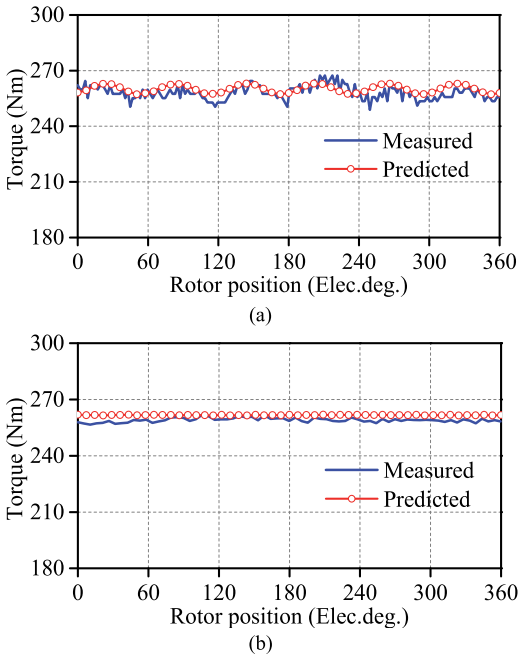

Fig. 26. Comparison of the measured and predicted torque waveform. (a) The $\alpha = 0°$ windings configuration. (b) The $\alpha = 30°$ windings configuration.

indicates the advantage of high windings factor. Moreover, the torque waveform of the $\alpha = 30°$ windings configuration is smoother than that of the $\alpha = 0°$ windings configuration, which is consistent with theoretical analysis. In addition, the current harmonics on torque performance are verified by the experiment, as shown in Fig. 27. Fig. 28 reveals the measured current spectrum, in which the 5th and 7th harmonics are existent,

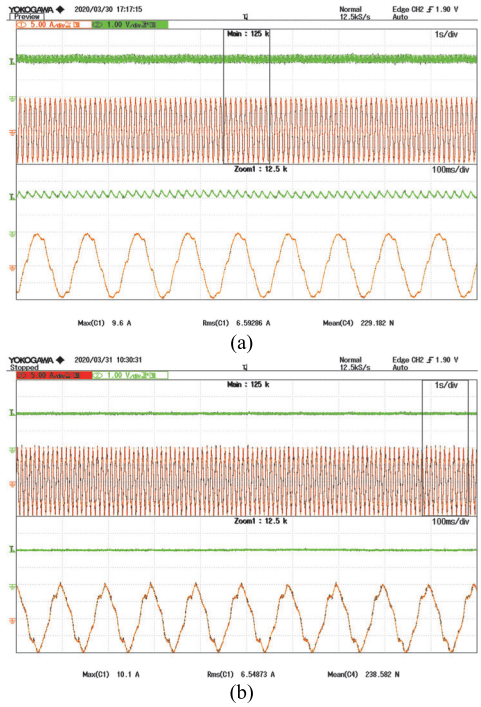

Fig. 27. Measured torque waveform with current harmonics. (100 ms/div, 5 A/div). (a) The α=0° windings configuration. (b) The α=30° windings configuration.

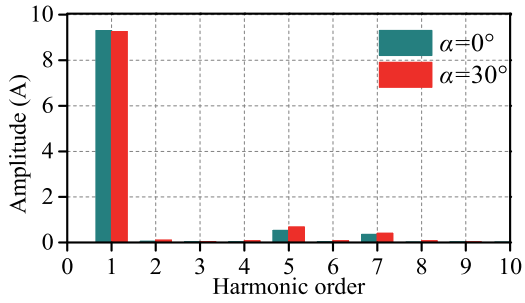

Fig. 28. Comparison of the related measured current spectrum.

and the amplitudes are similar. The torque waveform of the $\alpha = 30°$ windings configuration with current harmonics is smooth. However, the torque ripple of the $\alpha = 0°$ windings configuration increases obviously. This proves the torque harmonic generated by the 5th, 7th current harmonics can be eliminated when $\alpha = 30°$ for dual 3-phase windings.

Fig. 29 compares the measured efficiency map of the $\alpha = 0°$ windings and the $\alpha = 30°$ windings in the range of (20–260) r/min. Due to the high windings factor, the current value of the $\alpha = 30°$ windings is less than the $\alpha = 0°$ windings one. Therefore, the $\alpha = 30°$ windings exhibits higher efficiency than that of the $\alpha = 0°$ windings in full speed range. Specifically, the efficiencies of four different operating points are marked. It can be seen that the efficiency of the $\alpha = 30°$ windings increases by (0.6–1)% approximately, compared with the $\alpha = 0°$ windings ones.

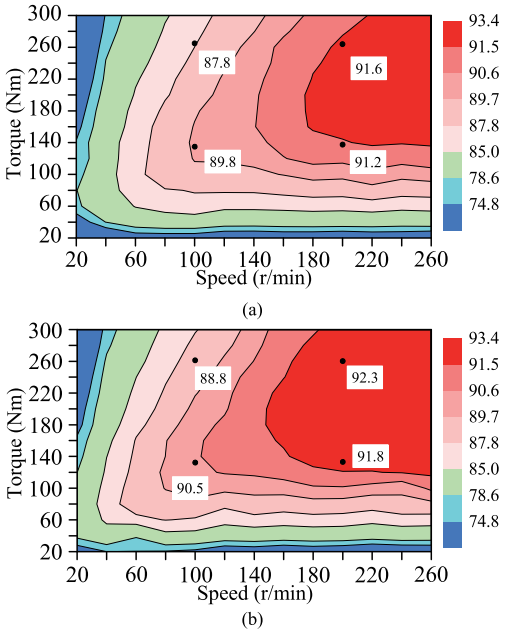

Fig. 29. Comparison of measured efficiency map. (a) The $\alpha = 0°$ windings configuration. (b) The $\alpha = 30°$ windings configuration.

V. Conclusion

In this paper, the torque improvement in dual *m*-phase windings configurations by phase shift for electric ship applications has been systematically studied. Firstly, the general relationship between the slot number and the phase number, which is appropriate for dual *m*-phase windings with different phase shifts, has been derived. Secondly, the effects of phase shift between adjacent windings set on torque capability have been investigated, and the optimal phase shift has been summarized in terms of reducing torque ripple, while improving the average torque. Furthermore, the 48-slot and 22-pole PM machine for electric ship has been designed and the optimal phase shift has been adopted. It is shown that the proposed windings configuration exhibits high average torque and low torque ripple. It has also been found the stator MMF harmonic components and radial force densities are improved. Finally, a prototype machine for electric ship has been built and tested, verifying that the dual *m*-phase windings with optimal phase shifts is effective to obtain better torque performance compared with its counterparts. This shows great potential in the electric ship applications.

References

[1] S. Fang, Y. Xu, Z. Li, T. Zhao, and H. Wang, "Two-step multi-objective management of hybrid energy storage system in all-electric ship microgrids," *IEEE Trans. Veh. Technol.*, vol. 68, no. 4, pp. 3361–3373, Apr. 2019.

[2] S. Fang, Y. Wang, B. Gou, and Y. Xu, "Toward future green maritime transportation: An overview of seaport microgrids and all-electric ships," *IEEE Trans. Veh. Technol.*, vol. 69, no. 1, pp. 207–219, Jan. 2020.

[3] M. Jaksic *et al.*, "Medium-voltage impedance measurement unit for assessing the system stability of electric ships," *IEEE Trans. Energy Convers.*, vol. 32, no. 2, pp. 829–841, Jun. 2017.

[4] K. Nounou, J. F. Charpentier, K. Marouani, M. Benbouzid, and A. Kheloui, "Emulation of an electric naval propulsion system based on a multiphase machine under healthy and faulty operating conditions," *IEEE Trans. Veh. Technol.*, vol. 67, no. 8, pp. 6895–6905, Aug. 2018.

[5] P. Ojaghlu and A. Vahedi, "Specification and design of ring winding axial flux motor for rim-driven thruster of ship electric propulsion," *IEEE Trans. Veh. Technol.*, vol. 68, no. 2, pp. 1318–1326, Feb. 2019.

[6] J. M. Crider and S. D. Sudhoff, "An inner rotor flux-modulated permanent magnet synchronous machine for low-speed high-torque applications," *IEEE Trans. Energy Convers.*, vol. 30, no. 3, pp. 1247–1254, Sep. 2015.

[7] Y. Luo, and C. Liu, "Pre- and post-fault tolerant operation of a six-phase PMSM motor using FCS-MPC without controller reconfiguration," *IEEE Trans. Veh. Technol.*, vol. 68, no. 1, pp. 254–263, Jan. 2019.

[8] W. Lee, J. H. Kim, W. Choi, and B. Sarlioglu, "Torque ripple minimization control technique of high-speed single-phase brushless DC motor for electric turbocharger," *IEEE Trans. Veh. Technol.*, vol. 67, no. 11, pp. 10357–10365, Nov. 2018.

[9] G. Xu, G. Liu, W. Zhao, Q. Chen, and X. Du, "Principle of torque-angle approaching in hybrid rotor permanent-magnet motor," *IEEE Trans. Ind. Electron.*, vol. 66, no. 4, pp. 2580–2591, Apr. 2019.

[10] G. Liu, X. Du, W. Zhao, and Q. Chen, "Reduction of torque ripple in inset permanent magnet synchronous machines by magnet shifting," *IEEE Trans. Magn.*, vol. 53, no. 2, Feb. 2017, Art. no. 8100713.

[11] Z. Wu, Z. Q. Zhu, C. Wang, J. C. Mipo, S. Personnaz, and P. Farah, "Reduction of open-circuit DC-winding-induced voltage in wound field switched flux machines by skewing," *IEEE Trans. Ind. Electron.*, vol. 66, no. 3, pp. 1715–1726, Mar. 2019.

[12] V. S.-Sempere, M. B.-Payan, and J.-R. C.-Bueno, "Cogging torque cancellation by magnet shaping in surface-mounted permanent-magnet motors," *IEEE Trans. Magn.*, vol. 53, no. 7, Jul. 2017, Art. no. 8107207.

[13] G. Liu, Y. Zeng, W. Zhao, and J. Ji, "Permanent magnet shape using analytical feedback function for torque improvement," *IEEE Trans. Ind. Electron.*, vol. 65, no. 6, pp. 4619–4630, Jun. 2018.

[14] X. Zhu, W. Hua, Z. Wu, W. Huang, H. Zhang, and M. Cheng, "Analytical approach for cogging torque reduction in flux-switching permanent magnet machines based on magnetomotive force-permeance model," *IEEE Trans. Ind. Electron.*, vol. 65, no. 3, pp. 1965–1979, Mar. 2018.

[15] Q. Chen, G. Xu, G. Liu, W. Zhao, L. Liu, and Z. Lin, "Torque ripple reduction in five-phase IPM machines by lowering interactional MMF," *IEEE Trans. Ind. Electron.*, vol. 65, no. 11, pp. 8520–8531, Nov. 2018.

[16] K. Wang, J. Zhang, Z. Gu, H. Sun, and Z. Q. Zhu, "Torque improvement of dual three-phase permanent magnet machine using zero sequence components," *IEEE Trans. Magn.*, vol. 53, No. 11, Nov. 2017, Art. no. 8109004.

[17] Y. Luo and C. Liu, "A simplified model predictive control for a dual three-phase PMSM with reduced current harmonics," *IEEE Trans. Ind. Electron.*, vol. 65, no. 11, pp. 9079–9089, Nov. 2018.

[18] Y. Li, Z. Q. Zhu, and G. Li, "Influence of stator topologies on average torque and torque ripple of fractional-slot SPM machines with fully closed slots," *IEEE Trans. Ind. Appl.*, vol. 54, no. 3, pp. 2151–2164, May/Jun. 2018.

[19] P. Xu *et al.*, "Analysis of dual three-phase permanent-magnet synchronous machines with different angle displacements," *IEEE Trans. Ind. Electron.*, vol. 65, no. 3, pp. 1941–1954, Mar. 2018.

[20] W. Zhao, J. Zheng, J. Ji, S. Zhu, and M. Kang, "Star and delta hybrid connection of fraction-slot concentrated-windings PM machine for low space harmonics," *IEEE Trans. Ind. Electron.*, vol. 65, no. 12, pp. 9266–9279, Dec. 2018.

[21] A. S. Abdel-Khalik, S. Ahmed, and A. Massoud, "Low space harmonics cancellation in double layer fractional slot windings using dual multi-phase windings," *IEEE Trans. Magn.*, vol. 51, no. 5, May 2015, Art. no. 8104710.

[22] Y. Demir and M. Aydin, "A novel asymmetric and unconventional stator windings configuration and placement for a dual three-phase surface PM machines," *IEEE Trans. Magn.*, vol. 53, no. 11, Nov. 2017, Art. no. 8111805.

[23] Y. Demir and M. Aydin, "A novel dual three-phase permanent magnet synchronous machines with asymmetric stator windings," *IEEE Trans. Magn.*, vol. 52, no. 7, Jul. 2016, Art. no. 8105005.

[24] L. Shao *et al.*, "Investigation on phase shift between multiple multiphase windings in flux-switching permanent magnet machines," *IEEE Trans. Ind. Appl.*, vol. 53, no. 3, pp. 1958–1970, May/Jun. 2017.

[25] Y. Hu, Z. Q. Zhu, and M. Odavic, "Torque capability enhancement of dual three-phase PMSM drive with fifth and seventh current harmonics injection," *IEEE Trans. Ind. Appl.*, vol. 53, no. 5, pp. 4526–4535, Sep./Oct. 2017.

[26] Z. Gu, K. Wang, Z. Q. Zhu, Z. Wu, C. Liu, and R. Cao, "Torque improvement in five-phase unequal tooth SPM machine by injecting third harmonic current," *IEEE Trans. Veh. Technol.*, vol. 67, no. 1, pp. 206–215, Jan. 2018.

[27] L. Alberti, and N. Bianchi, "Theory and design of fractional-slot multilayer windings," *IEEE Trans. Ind. Appl.*, vol. 49, no. 2, pp. 841–849, Mar./Apr. 2013.

[28] A. S. Abdel-Khalik, S. Ahmed, and A. M. Massoud, "Effect of multilayer windings with different stator winding connections on interior PM machines for EV applications," *IEEE Trans. Magn.*, vol. 52, no. 2, Feb. 2016, Art. no. 8100807.
[29] K. Wang, Z. Q. Zhu, Y. Ren, and G. Ombach, "Torque improvement of dual three-phase permanent-magnet machine with third-harmonic current injection," *IEEE Trans. Ind. Electron.*, vol. 62, no. 11, pp. 6833–6844, Nov. 2015.
[30] G. Feng, C. Lai, M. Kelly, and Narayan C. Kar, "Dual three-phase PMSM torque modeling and maximum torque per peak current control through optimized harmonic current injection," *IEEE Trans. Ind. Electron.*, vol. 66, no. 5, pp. 3356–3368, May 2019.
[31] K. Wang, "Effects of harmonics into magnet shape and current of dual three-phase permanent magnet machine on output torque capability" *IEEE Trans. Ind. Electron.*, vol. 65, no. 11, pp. 8758–8767, Nov. 2018.
[32] F. Chai, Y. Li, Y. Pei, and Y. Yu, "Analysis of radial vibration caused by magnetic force and torque pulsation in interior permanent magnet synchronous motors considering air-gap deformations," *IEEE Trans. Ind. Electron.*, vol. 66, no. 9, pp. 6703–6714, Sep. 2019.
[33] Y. Yokoi, T. Higuchi, and Y. Miyamoto, "General formulation of windings factor for fractional-slot concentrated windings design," *IET Electr. Power Appl.*, vol. 10, no. 4, pp. 231–239, Jan. 2016.
[34] X. Chen, J. Wang, and V. I. Patel, "A generic approach to reduction of magnetomotive force harmonics in permanent-magnet machines with concentrated multiple three-phase windings," *IEEE Trans. Magn.*, vol. 50, no. 11, Nov. 2014, Art. no. 8103604.
[35] J. Zheng, W. Zhao, J. Ji, J. Zhu, C. Gu, and S. Zhu, "Design to reduce rotor losses in fault-tolerant permanent-magnet machines," *IEEE Trans. Ind. Electron.*, vol. 65, no. 11, pp. 8476–8487, Nov. 2018.

Yuhua Sun received the B.Sc. degree in electrical engineering from the Qilu University of Technology (Shandong Academy of Sciences), Jinan, China, in 2017. He is currently working toward the Ph.D. degree in electrical engineering at Jiangsu University, Zhenjiang, China. His research interests include machine design and electromagnetic field analysis.

Wenxiang Zhao(Senior Member, IEEE) received the B.Sc. and M.Sc. degrees from Jiangsu University, Zhenjiang, China, in 1999 and 2003, respectively, and the Ph.D. degree from Southeast University, Nanjing, China, in 2010, all in electrical engineering. He has been with Jiangsu University since 2003, where he is currently a Professor with the School of Electrical Information Engineering. From 2008 to 2009, he was a Research Assistant with the Department of Electrical and Electronic Engineering, University of Hong Kong, Hong Kong. From 2013 to 2014, he was a Visiting Professor with the Department of Electronic and Electrical Engineering, University of Sheffield, Sheffield, U.K. His current research interests include electric machine design, modeling, fault analysis, and intelligent control. He has authored and co-authored over 250 technical papers in these areas.

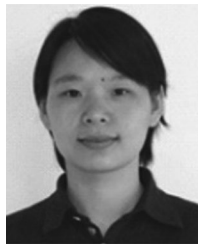

Jinghua Ji received the B.Sc., M.Sc., and Ph.D. degrees in electrical engineering from Jiangsu University, Zhenjiang, China, in 2000, 2003, and 2009 respectively. Since 2000, she has been with the School of Electrical and Information Engineering, Jiangsu University, where she is currently a Professor. From 2013 to 2014, she was a Visiting Scholar with the Department of Electronic and Electrical Engineering, University of Sheffield, Sheffield, U.K. Her areas of interest include motor design and electromagnetic field computation. She has authored and coauthored over 100 technical papers in these areas.

Junqiang Zheng received the B.Sc. degree in electrical engineering from Jiangsu University, Zhenjiang, China, in 2014, where he is currently working toward the Ph.D. degree in electrical engineering. His research interests include machine design and electromagnetic field computation.

Yu Cheng received the B.Sc. and M.Sc. degrees in electrical engineering from Jiangsu University, Zhenjiang, China, in 2017 and 2020 respectively. His research interests include control of linear permanent magnet vernier motor drive system.